Phase Locked Loop Based on an Observer for Grid Synchronization

Yongsoon Park and Seung-Ki Sul
Department of Electrical and Computer Engineering
Seoul National University
Seoul, Korea

Woo-Chull Kim
LG Uplus Corp.
Seoul, Korea

Hyun-Young Lee
PLASPO Co., Ltd.
Goyang City, Korea

***Abstract*—Grid synchronization technique is essential for grid-connected power converters. Phase locked loop (PLL) has been exploited as an implementation technique. However, additional efforts are required for PLL to deal with severely distorted grid voltages. In this paper, an observer is proposed to enhance the performance of PLL. A state equation is formulated to extract positive-sequence voltage from the distorted grid voltage and is utilized to construct the observer. Guidelines are suggested to set the gains of the observer along with its internal transfer functions. The PLL combined with the proposed observer has been tested in simulations and experiments in contrast to dual second order generalized integrator frequency locked loop (DSOGI-FLL). The results have validated that the proposed method reveals better phase-tracking performance for grid synchronization.**

I. INTRODUCTION

Electricity is delivered from suppliers to consumers via an electrical grid. The grid voltage is expected to be sinusoidal, whose frequency is fundamentally 50 or 60 Hz. This normal voltage is called as positive-sequence voltage. In particular, electrical power is mainly transferred by modulating the ac current corresponding to the positive-sequence voltage. It is useful to separate this 'positive-sequence fundamental power' from the rest of 'apparent power' [1].

The phase angle of grid voltage should be detected to elaborately modulate active and reactive powers when a grid-connected converter participates in power delivery. For this purpose, the method based on phase locked loop in the synchronous reference frame (SRF-PLL) has been widely used [2], [3]. However, because the grid voltage is usually polluted by unexpected distortions such as harmonics, unbalances, and glitches, the detection of its phase angle may not be easy with the simple PLL method.

Accordingly, a multitude of attempts have been made to detect the phase angle of positive-sequence voltage even under polluted grid conditions [4]-[6]. Namely, it is required to filter out any distortions except positive-sequence component for the accurate detection. Because each detection method has its own advantages and disadvantages, careful consideration is needed to select an appropriate method for grid synchronization. A proposed method in this paper is explicitly detailed in its construction and implementation. In addition, the effect of the proposed method is compared with conventional methods to obviously present its advantages.

In this paper, an observer is proposed as a preprocessing part of PLL to enhance the required performances for polluted grid conditions. In section II, it is described how the observer can obtain positive-sequence voltage without distortions. After the observer gains are specifically determined, the attachment of the observer to a PLL is detailed in section III. The proposed method is then assessed via simulation and experimental results under grid fault situations in section IV. Finally, the concluding remarks are noted in section V.

II. EXTRACTION OF POSITIVE-SEQUENCE VOLTAGES

A. Definitions of Symmetrical Components

In general, three-phase voltage can be decomposed into the symmetrical components: positive-, negative-, and zero-sequence voltages [7]. Initially, zero-sequence voltage cannot be measured in a three-wire three-phase grid, where only line-to-line voltages are accessible. In addition, negative-sequence voltage arises mainly when the grid is under abnormal operating conditions such as phase-to-ground faults and unbalanced loading conditions. In SRF-PLL, it is hard to filter out the negative-sequence voltage in the synchronous reference frame even though the bandwidth of PLL is reduced. [2], [4]. This negative-sequence voltage should be intensively considered for grid synchronization. Initially, positive sequence voltage can be defined as

$$\begin{cases} v_{a+} = -V_+ \sin\theta_p \\ v_{b+} = -V_+ \sin(\theta_p - 120°) \\ v_{c+} = -V_+ \sin(\theta_p + 120°) \end{cases} \quad (1)$$

where both the subscripts '+' and 'p' refer to positive-sequence, and θ_p is the phase angle of positive-sequence voltage.

As per the definition of (1), the positive-sequence voltage only exists in the quadrature axis of the synchronous reference frame. This definition has been adopted to maintain the coherence between grid and ac-motor applications. By using the same phase angle, negative sequence voltage can then be generalized into

978-1-4673-4355-8/13/$31.00 ©2013 IEEE

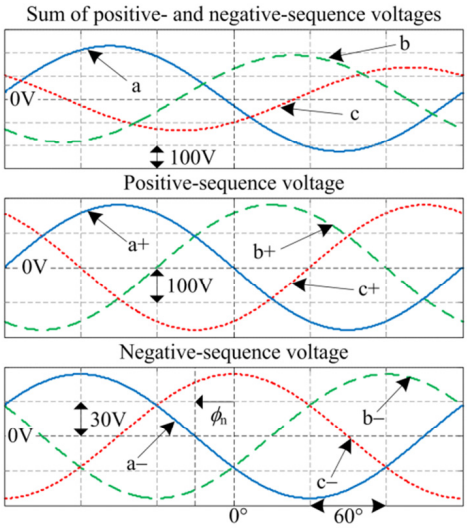

Figure 1. Positive- and negative-sequence votlages.

$$\begin{cases} v_{a-} = -V_- \sin(\theta_p + \phi_n) \\ v_{b-} = -V_- \sin(\theta_p + \phi_n + 120°) \\ v_{c-} = -V_- \sin(\theta_p + \phi_n - 120°) \end{cases} \quad (2)$$

where the subscript '–' represents negative-sequence, and ϕ_n is the phase difference of negative-sequence voltage to positive-sequence voltage.

For example, each voltage in (1) and (2) can be depicted in terms of the phase angle as shown in Fig. 1. In the figure, V_+ in (1) was set to 179.6 V, and V_- in (2) was 30 % of V_+. In addition, ϕ_n in (2) was set to 30 °.

B. An Observer for Estimating Positive-Sequence Voltage

For the observer design, the state equation on grid voltage must be established first. This state equation explains the relationship between states and their derivatives. That is, grid voltage should be discussed with respect to its time-variation. In particular, grid voltage can be considered in the synchronous reference frame by the Park's transformation:

$$\begin{bmatrix} v_d \\ v_q \end{bmatrix} = \frac{2}{3} \begin{bmatrix} \cos\hat{\theta}_p & \cos(\hat{\theta}_p - 120°) & \cos(\hat{\theta}_p + 120°) \\ -\sin\hat{\theta}_p & -\sin(\hat{\theta}_p - 120°) & -\sin(\hat{\theta}_p + 120°) \end{bmatrix} \begin{bmatrix} v_a \\ v_b \\ v_c \end{bmatrix} \quad (3)$$

where the hat '^' refers to estimated value hereafter.

For each phase, the sum of (1) and (2) can be inserted into the left-side of (3). Zero-sequence voltage is not considered because it is naturally erased in the process of (3). The d-q voltages can also be decomposed into positive- and negative-sequence components in the synchronous reference frame:

$$\begin{bmatrix} v_d \\ v_q \end{bmatrix} = \begin{bmatrix} v_{d+} \\ v_{q+} \end{bmatrix} + \begin{bmatrix} v_{d-} \\ v_{q-} \end{bmatrix} = \begin{bmatrix} -V_+ \sin\theta_d \\ V_+ \cos\theta_d \end{bmatrix} + \begin{bmatrix} -V_- \sin(2\hat{\theta}_p + \theta_d + \phi_n) \\ -V_- \cos(2\hat{\theta}_p + \theta_d + \phi_n) \end{bmatrix} \quad (4)$$

where $\theta_d = \theta_p - \hat{\theta}_p$. (5)

If $d\theta_d/dt$ and $d\phi_n/dt$ are negligible under the assumption of slow variation of the estimation error and the phase difference, the derivative of (4) can be approximated by the chain rule into

$$\frac{d}{dt}\begin{bmatrix} v_d \\ v_q \end{bmatrix} \approx \frac{d}{dt}\begin{bmatrix} v_{d-} \\ v_{q-} \end{bmatrix} = 2\frac{d}{dt}\hat{\theta}_p \cdot \begin{bmatrix} -V_- \cos(2\hat{\theta}_p + \theta_d + \phi_n) \\ V_- \sin(2\hat{\theta}_p + \theta_d + \phi_n) \end{bmatrix}. \quad (6)$$

Each negative-sequence component in (4) is repeated in the other axis of (6). Equation (6) is then rearranged into

$$\frac{d}{dt}\begin{bmatrix} v_d \\ v_q \end{bmatrix} \approx 2\frac{d}{dt}\hat{\theta}_p \cdot \begin{bmatrix} v_{q-} \\ -v_{d-} \end{bmatrix} = 2\hat{\omega}_p \begin{bmatrix} v_q - v_{q+} \\ v_{d+} - v_d \end{bmatrix} \quad (7)$$

where ω symbolizes frequency.

In (7), the derivatives of d-q voltages are explained with respect to themselves and their positive-sequence components. In addition, because it has been assumed to derive (7) that $d\theta_d/dt$ is small enough, the time-variations of positive-sequence components in (4) are considered to be negligible. Then, the state equation of the grid voltage can be derived as

$$\frac{d}{dt}V_s = \begin{bmatrix} 0 & 2\hat{\omega}_p & 0 & -2\hat{\omega}_p \\ -2\hat{\omega}_p & 0 & 2\hat{\omega}_p & 0 \\ 0 & 0 & 0 & 0 \\ 0 & 0 & 0 & 0 \end{bmatrix} V_s = A_m V_s \quad (8\text{-a})$$

$$V_o = \begin{bmatrix} v_d \\ v_q \end{bmatrix} = \begin{bmatrix} 1 & 0 & 0 & 0 \\ 0 & 1 & 0 & 0 \end{bmatrix} V_s = C_m V_s \quad (8\text{-b})$$

$$V_s = \begin{bmatrix} v_d & v_q & v_{d+} & v_{q+} \end{bmatrix}^T \quad (8\text{-c})$$

where the subscripts 's' and 'o' refer to state and output, respectively.

A Luenburger observer can be designed as (9) to estimate the internal states, v_{d+} and v_{q+}, because the system is observable with A_m and C_m in (8) [9]:

$$\frac{d}{dt}\hat{V}_s = A_m \hat{V}_s + L_m \cdot [V_o - C_m \hat{V}_s] \quad (9\text{-a})$$

$$L_m = \begin{bmatrix} p_1 & p_3 & q_1 & q_3 \\ p_2 & p_4 & q_2 & q_4 \end{bmatrix}^T \quad (9\text{-b})$$

$$\hat{V}_s = \begin{bmatrix} \hat{v}_d & \hat{v}_q & \hat{v}_{d+} & \hat{v}_{q+} \end{bmatrix}^T \quad (9\text{-c})$$

where variables in L_m are observer gains.

C. Gain Settings for the Observer

The observer gains of L_m in (9) must be specified to implement the observer. It follows which factors are considered to set the observer gains. Initially, the overall operation of the observer can be explained with its internal transfer functions in the Laplace domain. The state equation in (9) can be transformed into (10) when the derivative operator is replaced with the Laplace operator:

$$s \cdot \hat{V}_s = A_m \hat{V}_s + L_m \cdot [V_o - C_m \hat{V}_s]. \quad (10)$$

Equation (10) can be rearranged in terms of V_o:

$$\hat{V}_s = [s \cdot I_m - A_m + L_m C_m]^{-1} \cdot L_m V_o \quad (11)$$

where I_m represents the identity matrix.

Hence, the estimated states in (9-c) can be expressed with respect to the measurable states in (8-b):

$$\begin{cases} \hat{v}_d &= A_t/P_t \cdot v_d + E_t/P_t \cdot v_q \\ \hat{v}_q &= B_t/P_t \cdot v_d + F_t/P_t \cdot v_q \\ \hat{v}_{d+} &= C_t/P_t \cdot v_d + G_t/P_t \cdot v_q \\ \hat{v}_{q+} &= D_t/P_t \cdot v_d + H_t/P_t \cdot v_q \end{cases} \quad (12)$$

where all transfer functions in (12) are detailed with

$$A_t = p_1 s^3 + \{2\hat{\omega}_p(p_3 - q_3) + p_1 p_4 - p_2 p_3\}s^2 + 2\hat{\omega}_p(p_1 q_2 - p_2 q_1 + p_3 q_4 - p_4 q_3 + 2\hat{\omega}_p q_1)s + 4\hat{\omega}_p^2(q_1 q_4 - q_2 q_3) \quad (13\text{-a})$$

$$B_t = p_3 s^3 + 2\hat{\omega}_p(q_1 - p_1)s^2 + 4\hat{\omega}_p^2 q_3 s \quad (13\text{-b})$$

$$C_t = q_1 s^3 + (p_4 q_1 - p_3 q_2)s^2 + 2\hat{\omega}_p(p_1 q_2 - p_2 q_1 + 2\hat{\omega}_p q_1)s + 4\hat{\omega}_p^2(q_1 q_4 - q_2 q_3) \quad (13\text{-c})$$

$$D_t = q_3 s^3 + (p_4 q_3 - p_3 q_4)s^2 + 2\hat{\omega}_p\{q_3(q_2 - p_2) + q_4(p_1 - q_1) + 2\hat{\omega}_p q_3\}s \quad (13\text{-d})$$

$$E_t = p_2 s^3 + 2\hat{\omega}_p(p_4 - q_4)s^2 + 4\hat{\omega}_p^2 q_2 s \quad (13\text{-e})$$

$$F_t = p_4 s^3 + \{2\hat{\omega}_p(q_2 - p_2) + p_1 p_4 - p_2 p_3\}s^2 + 2\hat{\omega}_p(p_1 q_2 - p_2 q_1 + p_3 q_4 - p_4 q_3 + 2\hat{\omega}_p q_4)s + 4\hat{\omega}_p^2(q_1 q_4 - q_2 q_3) \quad (13\text{-f})$$

$$G_t = q_2 s^3 + (p_1 q_2 - p_2 q_1)s^2 + 2\hat{\omega}_p\{q_2(p_3 - q_3) + q_1(q_4 - p_4) + 2\hat{\omega}_p q_2\}s \quad (13\text{-g})$$

$$H_t = q_4 s^3 + (p_1 q_4 - p_2 q_3)s^2 + 2\hat{\omega}_p(p_3 q_4 - p_4 q_3 + 2\hat{\omega}_p q_4)s + 4\hat{\omega}_p^2(q_1 q_4 - q_2 q_3) \quad (13\text{-h})$$

$$\begin{aligned} P_t &= \det[s \cdot I_m - A_m + L_m C_m] \\ &= s^4 + (p_1 + p_4)s^3 + 4\hat{\omega}_p^2(q_1 q_4 - q_2 q_3) \\ &\quad + \{4\hat{\omega}_p^2 + 2\hat{\omega}_p(p_3 - p_2 + q_2 - q_3) + p_1 p_4 - p_2 p_3\}s^2 \\ &\quad + 2\hat{\omega}_p\{p_1 q_2 - p_2 q_1 + p_3 q_4 - p_4 q_3 + 2\hat{\omega}_p(q_1 + q_4)\}s \end{aligned} \quad (14)$$

Among the transfer functions in (12), most important factors are C_t/P_t and H_t/P_t, which explain the influence of each axis voltage to its estimated positive-sequence voltage. Therefore, this paper crucially considers these functions to set the observer gains. Initially, the roll-off rate of C_t/P_t and H_t/P_t can simply be increased by setting q_1 and q_4, the highest order coefficients in the numerators, to zero:

$$q_1 = q_4 = 0 . \quad (15)$$

The settings of (15) are intended to enhance the filtering performance to high-frequency distortions. With (15), C_t and H_t are simplified into

$$C_t = -p_3 q_2 s^2 + 2\hat{\omega}_p p_1 q_2 s - 4\hat{\omega}_p^2 q_2 q_3 \quad (16)$$

$$H_t = -p_2 q_3 s^2 - 2\hat{\omega}_p p_4 q_3 s - 4\hat{\omega}_p^2 q_2 q_3 . \quad (17)$$

To prevent non-minimum phase responses, all the coefficients must have the same sign in each of (16) and (17). This condition causes the roots of each equation to be placed in the left half plane (LHP) and is presented as

$$p_1 / p_3 < 0,\ q_3 / p_3 > 0,\ p_4 / p_2 > 0,\ q_2 / p_2 > 0 . \quad (18)$$

Meanwhile, the observer poles can be determined by using the concept of general second order system as follows:

$$P_{set} = (s^2 + 2\zeta_1\omega_{n1}s + \omega_{n1}^2)(s^2 + 2\zeta_2\omega_{n2}s + \omega_{n2}^2) \quad (19)$$

where ζ_x is damping ratio, and ω_{nx} is natural frequency.

After the damping ratios and the natural frequencies are determined, the observer gains are set by comparing the coefficients between (14) and (19). Considering that all the coefficients are positive in (19), the condition in (20) must be satisfied in the coefficient comparison after (15) is applied:

$$p_1 + p_4 > 0,\ q_2 q_3 < 0 . \quad (20)$$

Next design point is to set the observer gains so that the observer structure is symmetric. This can contribute to the simple implementation of the observer because similar gains can be repeated. The symmetric structure can be achieved with (21) when the conditions of (15), (18), and (20) are assumed:

$$p_1 = p_4,\ p_2 = -p_3,\ q_2 = -q_3 . \quad (21)$$

By the settings of (15) and (21), the equations of (13) and (14) are simplified into (22) and (23), respectively:

$$A_t = F_t = p_1 s^3 + \{2\hat{\omega}_p(q_2 - p_2) + p_1^2 + p_2^2\}s^2 + 4\hat{\omega}_p p_1 q_2 s + 4\hat{\omega}_p^2 q_2^2 \quad (22\text{-a})$$

$$B_t = -E_t = -(p_2 s^3 + 2\hat{\omega}_p p_1 s^2 + 4\hat{\omega}_p^2 q_2 s) \quad (22\text{-b})$$

$$C_t = H_t = p_2 q_2 s^2 + 2\hat{\omega}_p p_1 q_2 s + 4\hat{\omega}_p^2 q_2^2 \quad (22\text{-c})$$

$$D_t = -G_t = -\{q_2 s^3 + p_1 q_2 s^2 + 2\hat{\omega}_p q_2(q_2 - p_2 + 2\hat{\omega}_p)s\} \quad (22\text{-d})$$

$$P_t = s^4 + 2p_1 s^3 + \{4\hat{\omega}_p^2 + 4\hat{\omega}_p(q_2 - p_2) + p_1^2 + p_2^2\}s^2 + 4\hat{\omega}_p p_1 q_2 s + 4\hat{\omega}_p^2 q_2^2 . \quad (23)$$

The observer gains in (23) can then be specified with respect to predetermined damping ratios and natural frequencies in (19) by the coefficient comparison. Because harmonic distortions commonly occur at multiples of fundamental frequency, it would be convenient to set the natural frequency to be proportional to the grid frequency:

$$\omega_{n1} = k_1\hat{\omega}_p,\ \omega_{n2} = k_2\hat{\omega}_p \quad (24)$$

where $\hat{\omega}_p$ is estimated fundamental frequency. It is noticeable that $\hat{\omega}_p$ has already been used for the observer design since (7).

With (21) and (24), the coefficient comparison between (19) and (23) results in

$$p_1 = p_4 = (\zeta_1 k_1 + \zeta_2 k_2)\hat{\omega}_p \quad (25)$$

$$4\hat{\omega}_p^2 + 4\hat{\omega}_p(q_2 - p_2) + p_1^2 + p_2^2 = (k_1^2 + k_2^2 + 4\zeta_1\zeta_2 k_1 k_2)\hat{\omega}_p^2 \quad (26)$$

$$4\hat{\omega}_p p_1 q_2 = 2k_1 k_2(\zeta_1 k_2 + \zeta_2 k_1)\hat{\omega}_p^3 \quad (27)$$

$$4\hat{\omega}_p^2 q_2^2 = k_1^2 k_2^2 \hat{\omega}_p^4 . \quad (28)$$

If p_1 in (25) is inserted into (27), q_2 is uniquely determined. This resultant q_2 must then satisfy (28). Equation (28) is rearranged into (29) by the insertion of the resultant q_2:

$$\left(\frac{\zeta_1 k_2 + \zeta_2 k_1}{\zeta_1 k_1 + \zeta_2 k_2}\right)^2 = 1 . \quad (29)$$

Because each value in (29) has been assumed to be positive, (29) is further simplified into

$$(\zeta_2 - \zeta_1)(k_1 - k_2) = 0 . \quad (30)$$

When the observer poles are placed according to (19), the gain settings of (15) and (21) are allowed to use only if (30) is satisfied. At least, one of two factors in (30) must be zero. Namely, when (26) is considered, (31) must be satisfied if ζ_1 is equal to ζ_2 while (32) does so if k_1 is equal to k_2:

$$(p_2/\hat{\omega}_p - 2)^2 = (k_1 - k_2)^2(1-\zeta_1^2) \tag{31}$$

$$(p_2/\hat{\omega}_p - 2)^2 = -k_1^2 \cdot (\zeta_1 - \zeta_2)^2 . \tag{32}$$

It is important to remind that every value is real number in (31) and (32). According to (31), k_1 and k_2 can be different under the constraint of (33) even if ζ_1 and ζ_2 are the same. However, ζ_1 must be identical to ζ_2 in (32) if k_1 is equal to k_2. Therefore, the setting for (31) is selected for more degree of freedom to place the observer poles.

$$(1-\zeta_1^2) \geq 0 \;\rightarrow\; -1 \leq \zeta_1 \leq 1 . \tag{33}$$

In a general second order system, oscillatory responses would occur if damping ratio is smaller than unity. Therefore, in (33), the damping ratio could be set to unity. With this configuration, the observer gains in (21) are finally specified from the coefficient comparison as

$$\begin{cases} p_1 = p_4 = (k_1 + k_2)\hat{\omega}_p \\ p_2 = -p_3 = 2\hat{\omega}_p \\ q_2 = -q_3 = k_1 k_2 \hat{\omega}_p / 2 \end{cases} . \tag{34}$$

D. Pole placements of the Observer

Considering (12) and (22), the estimated positive-sequence voltage is expressed with

$$\begin{cases} \hat{v}_{d+} = C_t/P_t \cdot v_d - D_t/P_t \cdot v_q \\ \hat{v}_{q+} = D_t/P_t \cdot v_d + C_t/P_t \cdot v_q \end{cases} . \tag{35}$$

The substitution of (36) is applied to make the transfer functions similar to the general second order system:

$$k_1 = k,\; k_2 = \rho k . \tag{36}$$

The transfer functions in (35) are then derived as (37) and (38) after reducing common denominators:

$$\frac{C_t}{P_t} = \frac{\rho(k\hat{\omega}_p)^2}{s^2 + (1+\rho)k\hat{\omega}_p s + \rho(k\hat{\omega}_p)^2} \tag{37}$$

$$\frac{D_t}{P_t} = -\frac{1}{2}\frac{\rho k^2 \hat{\omega}_p s}{s^2 + (1+\rho)k\hat{\omega}_p s + \rho(k\hat{\omega}_p)^2} . \tag{38}$$

When the gain ρ is set to 1, (37) becomes a general second order system with unity damping ratio, and the gain k contributes to the adjustment of bandwidth. The frequency responses of (37) and (38) are depicted in Fig. 2 when the gain k varies. As shown in Fig. 2, the gain k can adjust the attenuating ratio of the harmonics incorporated in grid voltage.

However, it is not explicit in (35) how the proposed observer can reject negative-sequence voltage. Considering (4), negative-sequence voltage can be expressed with (39) at two times the fundamental frequency in the synchronous reference frame:

$$\begin{bmatrix} v_{d-}(t) \\ v_{q-}(t) \end{bmatrix} = \begin{bmatrix} -V_- \sin(2\omega_p t) \\ -V_- \cos(2\omega_p t) \end{bmatrix} \xrightarrow{\mathcal{L}} v_{d-}(s) = \frac{2\omega_p}{s} v_{q-}(s) . \tag{39}$$

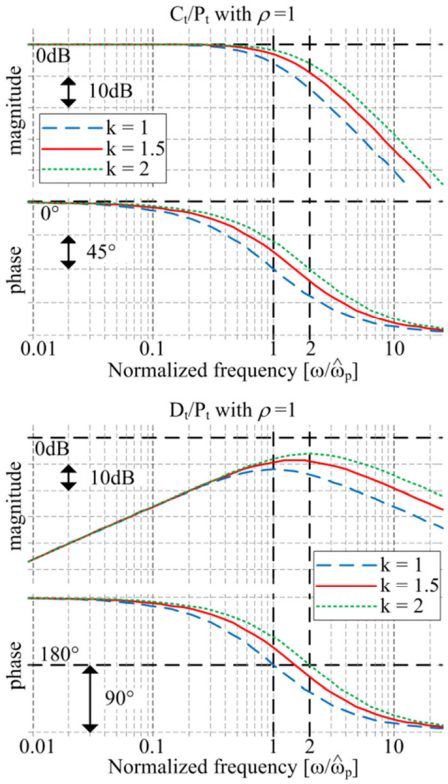

Figure 2. Bode plots of C_t/P_t and D_t/P_t.

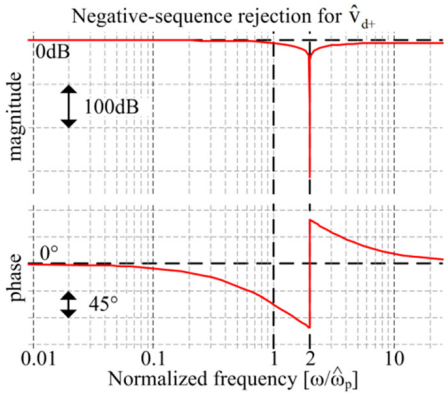

Figure 3. Negative-sequence rejection to estimate the d-axis positive-sequence voltage.

If $\hat{\omega}_p$, the estimated frequency, is assumed to be accurate, (35) can be rearranged into (40) in terms of the negative-sequence voltage of (39):

$$\begin{cases} \hat{v}_{d+}(s) = \dfrac{\rho k^2}{4}\dfrac{s^2 + 4\hat{\omega}_p^2}{(s + k\hat{\omega}_p)(s + \rho k\hat{\omega}_p)} \cdot v_{d-}(s) \\ \hat{v}_{q+}(s) = 0 \end{cases} . \tag{40}$$

As explicitly shown in (40), negative-sequence voltage cannot be reflected in the estimation of the q-axis positive-sequence voltage if the observer implementation is ideal. This sort of rejection can also be confirmed in the d-axis estimation when considering the d-axis transfer function. Its Bode plot is depicted in Fig. 3 when the gains ρ and k are 1 and 1.5, respectively. As shown in Fig. 3, the d-axis transfer function in (40) serves as a notch filter. The rejection-band in Fig. 3 is

determined by the numerator of the transfer function. Namely, if s is substituted with $j\cdot 2\,\hat{\omega}_p$ in (40), the band-rejection is easily proved. Therefore, for the rejection of negative-sequence voltage, the accuracy of $\hat{\omega}_p$ to the actual counterpart is crucial rather than the gains ρ and k.

III. PLL Based on the Observer

The observer proposed in section II is attached to SRF-PLL. By virtue of this construction, filtering harmonics can be readily achieved with less effort in the view point of PLL. This allows PLL to increase its bandwidth, which contributes to the higher phase-angle tracking dynamics. The entire PLL structure is shown in Fig. 4. Henceforth, this PLL structure is referred to as Synchronous Observer-Aided Preprocessing phase locked loop (SOAP-PLL).

The estimated frequency in PLL must be fed back to the observer because the state equation in (8) is fundamentally based on this value, which is also used to set the observer gains according to (34). Usually, ω_{e2} in Fig. 4 has been used as estimated frequency. However, ω_{e2} may be sensitive to distortions because k_{pp}, the proportional gain, directly delivers scaled angle errors to it. To refine this drawback, ω_{e1} in Fig. 4 is used for the observer. The effectiveness of this modification can be discussed with following equations. When (41) is assumed, (42) can be derived from Fig. 4:

$$\hat{\theta}_d \approx \theta_d = \theta_p - \hat{\theta}_p \tag{41}$$

$$\hat{\theta}_p = \frac{k_{pp}s + k_{ip}}{s^2 + k_{pp}s + k_{ip}}\theta_p \tag{42}$$

where k_{pp} and k_{ip} are proportional and integral (PI) gains for PLL.

From Fig. 4 with (41), ω_{e1} is derived as

$$\omega_{e1} = \frac{k_{ip}}{s}\hat{\theta}_d \approx \frac{k_{ip}}{s}(\theta_p - \hat{\theta}_p). \tag{43}$$

If $\hat{\theta}_p$ in (42) is inserted into (43), it can be rearranged into

$$\omega_{e1} \approx \frac{k_{ip}s}{s^2 + k_{pp}s + k_{ip}}\theta_p = \frac{k_{ip}}{s^2 + k_{pp}s + k_{ip}}\omega_p. \tag{44}$$

That is, ω_{e1} is a low-pass filtered value of actual frequency. By using this frequency as $\hat{\omega}_p$, the observer performance can be less sensitive to distortions. In addition, because the transfer function in (44) takes the form of general second order system, the PI gains can be set according to the setting rules of the second order system:

$$k_{pp} = 2\zeta_{pll}\omega_{npll},\ k_{ip} = \omega_{npll}^2 \tag{45}$$

where ζ_{pll} and ω_{npll} are respectively damping ratio and natural frequency of PLL.

The gain settings of the observer and PLL have to come together. In this paper, all the gains are set so that the bandwidth of (37) is larger enough than that of (42). That is, if the dominant pole of observer is not large enough to that of PLL, the dynamics intended in (42) would be disturbed.

Meanwhile, based on the equation obtained from dividing both sides of (10) by 's,' the proposed observer can be specifically implemented as shown in Fig. 5. In the process of

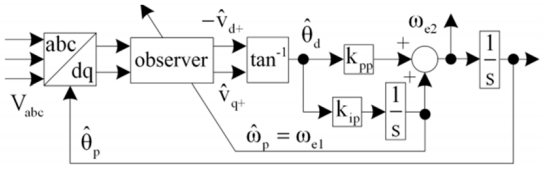

Figure 4. Entire PLL structure.

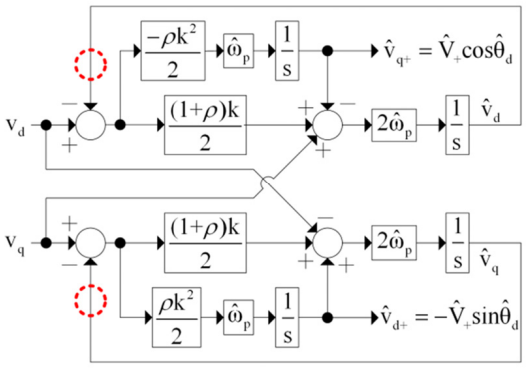

Figure 5. Block diagram of the proposed observer.

obtaining Fig. 5, the observer gains have been set according to (15), (34), and (36). Even though the derivation and description of the observer gains seem to be rather complicated, the practical implementation of the proposed observer is simple enough as shown in Fig. 5.

IV. Simulation and Experimental Results

A. Evaluation of SOAP-PLL

The performance of SOAP-PLL can be discussed in two aspects, the tracking error on grid parameters and the mitigating ability against distortions. Each performance has been examined under grid faults, where the grid voltages were contaminated by harmonics and unbalances, and the fundamental frequency was changed.

In particular, the effectiveness of SOAP-PLL is discussed with the comparison to a conventional method, dual second order generalized integrator frequency locked loop (DSOGI-FLL). This DSOGI-FLL has been selected because its implementation is relatively simple, and essential gain settings have been explicitly known [5].

B. Simulation Results

The fault conditions for simulation tests have been quoted from the literature [10]. When the voltage amplitude at ideal grid is selected as the base voltage, the phasor of the normal voltage is denoted as $1\angle 0°$. Based on this concept, the fault conditions are given as follows:

$$V_{1+} = 0.5\angle -30°,\ V_{1-} = 0.25\angle 110° \tag{46}$$

$$V_{5-} = 0.2\angle 0°, V_{7+} = 0.2\angle 0°, V_{11-} = 0.2\angle 0° \tag{47}$$

$$f_{fault} - f_{nor} = -5\,\text{Hz} \tag{48}$$

where the subscript number of a voltage represents harmonic order, and normal condition is indicated by the subscript 'nor'.

When the normal grid is assumed to be $220V_{rms}$-60Hz, and all the conditions in (46), (47), and (48) are applied after fault, fault waveforms can be depicted as shown in Fig. 6.

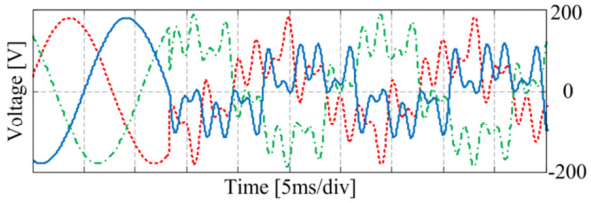

Figure 6. Grid fault under conditions of (46), (47), and (48).

Initially, the gains of DSOGI-FLL were set according to the earlier work [5]. For the fair comparison in performances, the gains of SOAP-PLL had to be set such that its dynamics was similar to that of DSOGI-FLL under the unbalance fault of (46). The specific values of those gains were

$$\rho = 1,\ k = 1.7,\ \zeta_{pll} = 1,\ \omega_{npll} = 2\pi \cdot 20\ . \tag{49}$$

The gains of ρ and k are directly inserted into the observer of Fig. 5, and the gains of ζ_{pll} and ω_{npll} are reflected in the PLL of Fig. 4 via the PI gains in (45). With these specific values, SOAP-PLL has presented the same settling time under the condition of (46) only, as shown in Fig. 7.

Due to the step variations in (46), the estimation errors of phase angle and frequency present oscillations for a while after the fault, as captured in Fig. 7. However, after the oscillations disappear, both methods shows perfect grid synchronizations as if there are no unbalance distortions. This result confirms that the unbalance rejection of SOAP-PLL is comparable with that of DSOGI-FLL.

The performance of SOAP-PLL was different to that of DSOGI-FLL when each method was implemented in discrete time domain, or the harmonics in (47) were included in fault conditions. In the digital implementation, every integrator in both methods was implemented with the backward Euler method, which is the simplest method for digitization [11], [12]. With this digital implementation, each method for grid synchronization was tested under the fault conditions of (46), (47), and (48). The result is presented in Fig. 8.

As shown in Fig. 8, SOAP-PLL obviously outperforms DSOGI-FLL in harmonic filtering. This is because SOAP-PLL consists of two filtering stages, the observer and PLL. Even though the filtering performance of DSOGI-FLL can be further improved through the extension to multiple SOGI-FLL (MSOGI-FLL) [10], this extension must pay with the increment of source codes for implementation. In addition, the frequency of DSOGI-FLL presents the average error of 0.79 Hz mainly due to harmonics.

The other conspicuous feature is that DSOGI-FLL shows the steady-state error of 2.7 ° in estimating phase angle. To explain this phenomenon, one of dual SOGI is shown in Fig. 9. To estimate positive-sequence voltage, the followings are important in Fig. 9:

$$D(s) = \frac{k\hat{\omega}_p s}{s^2 + k\hat{\omega}_p s + \hat{\omega}_p^2} = \frac{\hat{v}_\alpha}{v_\alpha} \tag{50-a}$$

$$Q(s) = \frac{k\hat{\omega}_p^2}{s^2 + k\hat{\omega}_p s + \hat{\omega}_p^2} = \frac{q\hat{v}_\alpha}{v_\alpha} \tag{50-b}$$

where the subscript 'α' refers to d-axis in the stationary reference frame. Q(s) particularly generates the quadrature

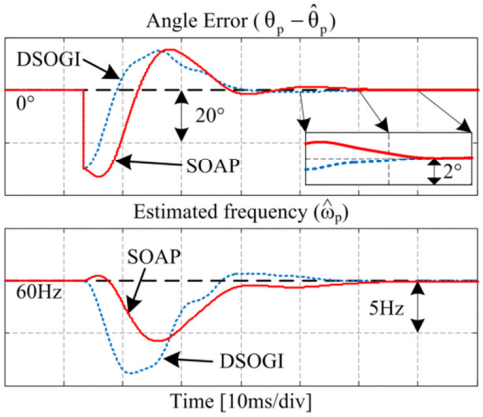

Figure 7. Simulation results under unbalance fault of (46) with analog implemenations.

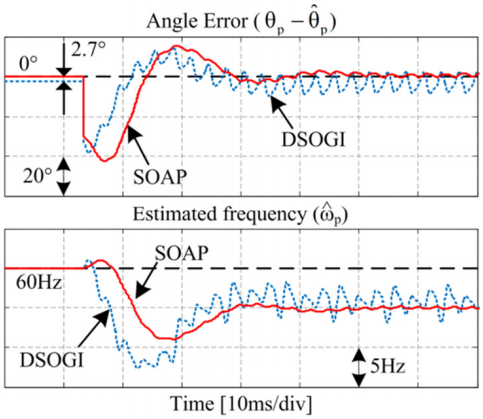

Figure 8. Simulation results under fault conditions of (46), (47), and (48) with digital implementations.

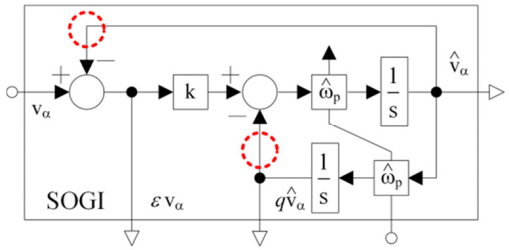

Figure 9. Second order generalized integrator.

signal of input while both D(s) and Q(s) serve filtering harmonics.

When a system is transformed from the s-domain to the z-domain, its property can be distorted. Moreover, the computational delay of z^{-1}, which is indicated by dashed circles in Figs. 5 and 9, may be included for feedback. To specify this distortion, the following concept is introduced in this paper, which is called as z-transformation distortion (ZTD):

$$ZTD_H(\omega) = \frac{H_z(e^{j\omega T_s})}{H_s(j\omega)} \tag{51}$$

where 'H' symbolizes the system itself of interest, H_s refers to the original system in the s-domain, and H_z represents the transformed system in the z-domain. In addition, ω is the frequency of concern, and T_s is the sampling frequency for digital implementation.

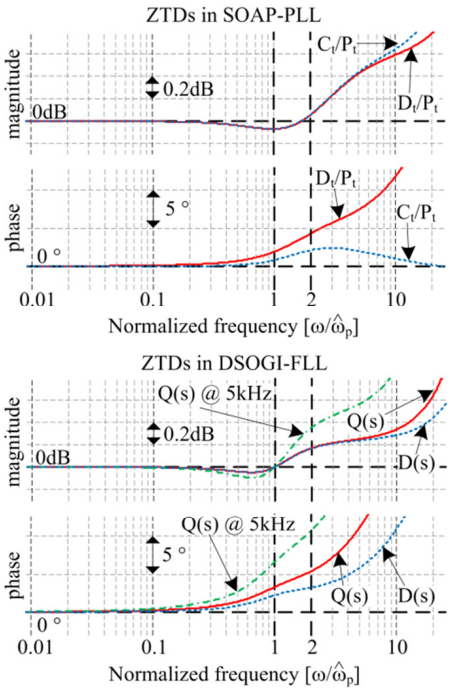

Figure 10. Bode plots of ZTDs in SOAP-PLL and DSOGI-FLL with 10kHz sampling.

The meaning of ZTD is the distorted degree of the z-domain system from the s-domain system. The Bode plot of ZTD corresponds to the differences between the Bode plots of each system:

$$20\log_{10}|\mathrm{ZTD}_{\mathrm{H}}(\omega)| = 20\log_{10}|\mathrm{H}_z(e^{j\omega T_s})| - 20\log_{10}|\mathrm{H}_s(j\omega)| \quad (52)$$

$$\angle\mathrm{ZTD}_{\mathrm{H}}(\omega) = \angle\mathrm{H}_z(e^{j\omega T_s}) - \angle\mathrm{H}_s(j\omega)\,. \quad (53)$$

The Bode plots of ZTDs in SOAP-PLL and DSOGI-FLL are depicted in Fig. 10 when the sampling frequency is set at 10 kHz. In the Bode plot of ZTD, magnitude and phase must be respectively 0 dB and 0 °, which corresponds to unity, when the z-transformation is ideal. As shown in Fig. 10, the ZTDs deviate from the unity when the frequency of concern approaches to the Nyquist frequency.

From Fig. 10, it can be explained why the steady-state error arises in DSOGI-FLL, and not in SOAP-PLL. To estimate phase angle, positive-sequence voltage must be estimated at the fundamental frequency in DSOGI-FLL. However, the ZTDs of D(s) and Q(s) exhibit the phase distortions of 2.2 and 3.2 degrees at that frequency. For ac components, these nonzero phases correspond to parallel displacements in time-domain. These displacements cause the steady-state error in DSOGI-FLL, and can be intensified at smaller sampling frequency as shown in Fig. 10 (denoted by @5kHz). In contrast, SOAP-PLL estimates positive-sequence voltage at dc band, where its ZTDs approach to the unity. Unlike SOAP-PLL, accurate digitizing strategy seems to be required for DSOGI-FLL rather than the simple backward Euler method [11]-[13].

In addition, the condition of (48) has also been included in the fault test of Fig. 8 to examine the frequency-adaptive property of SOAP-PLL. Because distortions are nearly not observed at two times the fundamental frequency in Fig. 8, it

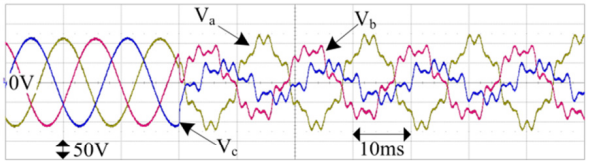

Figure 11. Grid fault for experiment.

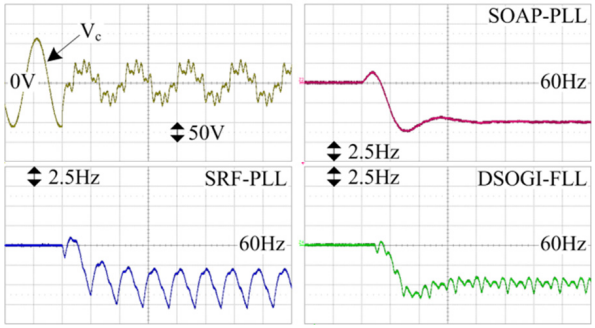

Figure 12. Frequency estimations in experiment: time [10ms/div].

can be recognized that SOAP-PLL successfully rejects negative-sequence voltage even after the frequency variation.

C. Experimental Results

To demonstrate the feasibility of SOAP-PLL, a grid fault was emulated using ac source, MX30. All algorithms were implemented in a digital signal processor (DSP), TMS320F28335, and grid voltages were sampled through voltage sensors per 100 μs. All the gains for SOAP-PLL were set according to (49).

The most frequent fault is the single phase-to-ground fault [14], which is commonly recognized as phase-to-phase fault by grid-connected converters due to transformers [8]. The phase-to-phase fault between b- and c-phases has been considered:

$$\begin{cases} \mathrm{V_a} = 1 \\ \mathrm{V_b} = -1/2 - j\mathrm{V_{sag}}\sqrt{3}/2 \\ \mathrm{V_c} = -1/2 + j\mathrm{V_{sag}}\sqrt{3}/2 \end{cases} \quad (54)$$

where $\mathrm{V_{sag}}$ is a complex number indicating the degree of voltage sag. In addition, all magnitudes are in per unit.

The magnitude of $\mathrm{V_{sag}}$ is determined according to the phase of $\mathrm{V_{sag}}$ [8]. For experiment, $\mathrm{V_{sag}}$ was set to $0.38\angle -40$ °. The magnitudes of harmonics at 5th, 7th, and 11th orders were set to about 0.08 per unit, and the frequency variation in (48) was included as well. The grid voltage around the fault occurrence has then been recognized in the DSP board as shown in Fig. 11.

Initially, the c-phase voltage, whose negative peak was the starting point of the fault, was selected as the reference to capture several waveforms due to the limited channels of oscilloscope. It was assumed that the ac source could generate almost time-invariant faults by the same settings.

Under the fault situation, SOAP-PLL has presented the least harmonics in the frequency estimation shown in Fig. 12. The effect of the proposed observer can be more obvious via the comparison with SRF-PLL, where only the observer part has been eliminated from SOAP-PLL. In particular, negative-

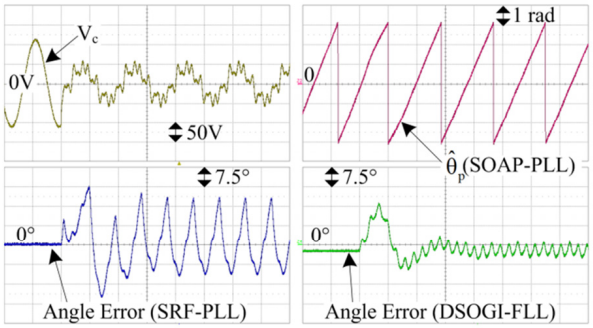

Figure 13. Angle estimations in experiment: time [10ms/div].

sequence distortions were evidently rejected by SOAP-PLL. After the estimations settled down, the RMS of frequency ripple was 0.1 Hz for SOAP-PLL, 1.52 Hz for SRF-PLL, and 0.45 Hz for DSOGI-FLL. Furthermore, the frequency of DSOGI-FLL presented the average deviation of 0.102 Hz when compared to SOAP-PLL.

Because the information of actual phase angle was not permitted to access, angle errors were calculated with respect to the phase angle of SOAP-PLL when considering the simulation result. After the estimations settled down, the phase angle of DSOGI-FLL deviated from that of SOAP-PLL by 2.4 ° as shown in Fig. 13.

V. CONCLUSION

In this paper, an observer has been proposed to clearly extract positive-sequence voltage from the polluted grid voltage. This extraction is intended to reinforce the function of PLL by using the observer as a preprocessor. The state equation has been newly derived on grid voltage to construct the observer, and the gain settings of the observer have been obviously suggested when considering the mitigation of grid distortions and the combination with PLL.

In functional aspect, the proposed PLL method was specifically scrutinized in terms of filtering harmonics and rejecting unbalances under polluted grid conditions when the dynamics to track the phase angle was adjusted to be similar to a conventional method. In particular, the performances were discussed in digitally implemented structures under the consideration of practical implementation. In result, the effectiveness of the proposed method has been confirmed by simulation and experimental results. Despite simple implementation, the proposed method excelled in mitigating distortions of the estimated frequency and phase angle without steady-state errors.

REFERENCES

[1] A. E. Emanuel, "Summary of IEEE Standard 1459: Definitions for the Measurement of Electric Power Quantities Under Sinusoidal, Nonsinusoidal, Balanced, or Unbalanced Conditions," IEEE Trans. Ind. Appl., vol. 40, no. 3, pp. 869-876, May/June 2004.

[2] S.-K. Chung, "A Phase Tracking System for Three Phase Utility Interface Inverters," IEEE Trans. Power Electron., vol. 15, no. 3, pp. 431-438, May 2000.

[3] V. Kaura and V. Blasko, "Operation of a Phase Locked Loop System Under Distorted Utility Conditions," IEEE Trans. Ind. Appl., vol. 33, no. 1, Jan./Feb. 1997.

[4] S.-J. Lee, H. Kim and S.-K. Sul, "A New Phase Detecting Method for Power Conversion Systems Considering Distorted Conditions in Power System," conf. rec. IEEE Ind. Appl. Conf, 1999, pp. 2167-2172.

[5] P. Rodriguez, A. Luna, R. S. Munoz-Aguilar, I. Etxeberria-Otadui, R. Teodorescu and F. Blaabjerg, "A Stationary Reference Frame Grid Synchronization System for Three-Phase Grid-Connected Power Converters Under Adverse Grid Conditions," IEEE Trans. Power Electron., vol. 27, no. 1, Jan. 2012.

[6] P. Rodriguez, J. Pou, J. Bergas, J. I. Candela, R. P. Burgos and D. Boroyevich, "Decoupled Double Synchronous Reference Frame PLL for Power Converters Control," IEEE Trans. Power Electron., vol. 22, no. 2, Mar. 2007.

[7] A. R. Bergen and V. Vittal, "Symmetrical Components" in *Power Systems Analysis 2nd edition*, Korea: Pearson Educ. Korea Ltd, 2009, ch. 12-1, pp. 446-450.

[8] A. Sannino, M. H. J. Bollen, and J. Svensson, "Voltage Tolerance Testing of Three-Phase Voltage Source Converters," IEEE Trans. Power Delivery, vol. 20, no. 2, pp. 1633-1639, April 2005.

[9] D. G. Luenberger, "An introduction to observers," IEEE Trans. Automatic Control, vol. 16, no. 6, pp. 596-602, Dec. 1971.

[10] P. Rodriguez, A. Luna, I. Candela, R. Mujal, R. Teodorescu and F. Blaabjerg, "Multiresonant Freuqency-Locked Loop for Grid Synchronization of Power Converters Under Distorted Grid Conditions," IEEE Trans. Ind. Electron., vol. 58, no. 1, Jan. 2011.

[11] A. G. Yepes, F. D. Freijedo, J. Doval-Gandoy, O. Lopez, J. Malvar and P. Fernandez-Comesana, "Effects of Discretization Methods on the Performance of Resonant Controllers," IEEE Trans. Power Electron., vol. 25, no. 7, July 2010.

[12] F. J. Rodriguez, E. Bueno, M. Aredes, L. G. B. Rolim, F. A. S. Neves and M. C. Cavalcanti, "Discrete-time implementation of second order generalized integrators for grid converters," Ann. Conf. IEEE Ind. Electron. (IECON), 2008, pp. 176-181.

[13] A. G. Yepes, F. D. FreiJedo, O. Lopez and J. Doval-Gandoy, "High-Performance Digital Resonant Controllers Implemented With Two Integrators," IEEE Trans. Power Electron., vol. 26, no. 2, Feb. 2011.

[14] J. Keller and B. Kroposki, "Understanding Fault Characteristics of Inverter-Based Distributed Energy Resources," NREL, Golden, CO, Tech. Rep. NREL/TP-550-46698, Jan. 2010.